



Opposite Atlantic Multidecadal Oscillation effects on dry/wet changes over Central and East Asian drylands



Shuyang Guo ^a, Xiaodan Guan ^{a,b,*}, Linlin Gao ^c, Wen Sun ^a, Chenyu Cao ^a, Yongli He ^{a,b}

^a Key Laboratory for Semi-Arid Climate Change of the Ministry of Education, College of Atmospheric Sciences, Lanzhou University, Lanzhou, Gansu, China

^b Collaborative Innovation Center for Western Ecological Safety, Lanzhou, Gansu, China

^c MOE Key Laboratory of Western China's Environmental Systems, College of Earth Environmental Sciences, Lanzhou University, Lanzhou, China

ARTICLE INFO

Keywords:

Atlantic Multidecadal Oscillation (AMO)
Dryland
Drought
Precipitation
Water-vapor transport

ABSTRACT

The Central Asian dryland (CAD) and East Asian dryland (EAD) are typical drylands in the globe. They are characterized by less precipitation, with vulnerable and sensitive ecosystems. Although they are located in the heart of continent, precipitation in these regions has opposite patterns on the multi-decadal time scale. In this study, we focus on different responses of precipitation changes in these drylands and related drought to different phases of the Atlantic Multidecadal Oscillation (AMO) on the multi-decadal time scale. We show that less precipitation in the CAD and more precipitation in the EAD were always associated with a positive AMO phase, which was caused by the weakened westerly and simultaneous enhancement of vertically integrated water vapor from the Indian Ocean and western Pacific. Such precipitation pattern was accompanied by a drying (wetting) phase of self-calibrating Palmer's drought severity index in the CAD (EAD), which further contributed to a worse (better) ecology in the CAD (EAD). This explains why the positive AMO phase in recent decades starting from 2000 made a positive contribution to the drying (wetting) arid region in the CAD (EAD).

1. Introduction

Drylands occupy approximately 40% of the global land, characterized by scarce rainfall, low soil water holding capacity and low nutrition content. Since about 1/3 of the world's population reside there, the ecosystems of drylands are more susceptible to human activities and climate change, due to poor self-restoration capability (Reed et al., 2012; Guan et al., 2016; Guo et al., 2018). The lack of water resources in drylands can directly influence the survival and development of human beings, and cause degradation of the ecosystems. The agriculture in drylands mainly depends on rainfall; and the available quantity of surface-water resources, a factor necessary to maintain agricultural irrigation, is rather sensitive to the change of precipitation (Liu and Xia, 2004; Schwinnning et al., 2004). Therefore, a small variation in dry-wet patterns can be calamitous (Guan et al., 2015; Huang et al., 2016).

Asian drylands stretch from the Caspian Sea in the west to Northeast China in the east, spanning approximately 40°–140°E and 30°–60°N (Wang et al., 2010; Huang et al., 2016). The climate in most of the Asian drylands tends to be wet and warm since the 1980s (Shi and Yu, 2003). There are remarkable differences in topography and climate change

between the Central Asian dryland (CAD; 40°–80°E and 30°–60°N) and East Asian dryland (EAD; 80°–140°E and 30°–60°N). As the largest arid region in the world, the CAD has an extensive mountain-oasis-desert and fragile ecological environment that is sensitive to changes of dry/wet condition (Chen and Huang, 2017; Zhang et al., 2019; Dilinuer et al., 2021). The CAD is the major part of Asian drylands, and is mainly covered by deserts (e.g., the Gobi Desert) and plateaus, which is influenced by the North Atlantic Oscillation and westerly circulation (Liu et al., 2018; Aizen et al., 2001). Additionally, surface air temperature has increased remarkably over the past few decades with global warming, and the warming trend is even more significant in the EAD. The EAD mainly includes the northeastern part of Kazakhstan, northern Mongolia, and parts of Northwest China; and it is covered by deserts, plains and grasslands, which are greatly affected by the South Asian summer monsoon and East Asian summer monsoon (EASM). Although the locations of these typical drylands are far away from the oceans, the global oceans play an important role in regional climate change in drylands (Hua and Ma, 2009; Guan et al., 2021). In particular, precipitation variation in some areas may be the result of oceanic decadal variability (e.g. McCabe et al., 2004; Sun et al., 2015; Si et al., 2020; Tao

* Corresponding author at: Key Laboratory for Semi-Arid Climate Change of the Ministry of Education, College of Atmospheric Sciences, Lanzhou University, Lanzhou, Gansu, China.

E-mail address: guanxd@lzu.edu.cn (X. Guan).

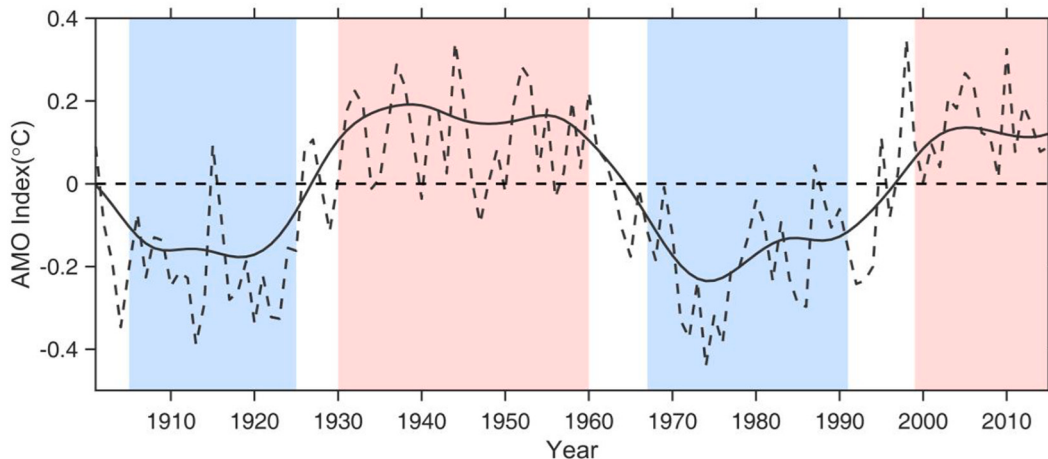


Fig. 1. Annual AMO index (dashed line) and filtered AMO index (solid line) during the period of 1901–2015. Red (blue) shading denotes the positive (negative) period of the AMO. (For interpretation of the references to colour in this figure legend, the reader is referred to the web version of this article.)

et al., 2021).

Dry-wet changes in drylands are significantly influenced by marine activities, especially sea-surface temperature (SST) anomalies in the Atlantic Ocean (Ting et al., 2011; Trenberth et al., 2014; Guan et al., 2019). The Atlantic Multidecadal Oscillation (AMO), a near-global-scale mode in the climate system, is one of the dominant oscillations of decadal climate variability, characterized by alternating warm and cold phases over large regions of the Northern Hemisphere with a period of 65–80 years (Jeff et al., 2006; Li and Gary, 2007; Lyu et al., 2017). Many studies have shown that the warm AMO phase is associated with local climate changes, such as increased precipitation over Sahel, less-than-normal precipitation over the Northwest Pacific (Mohino et al., 2011; Chen et al., 2015), enhancement of summer monsoon rainfall over India (Joshi and Pandey, 2011; Joshi and Ha, 2019), wetting over central America in summer, and drying over northeastern Brazil in winter, suggesting that the long-term predictability of drought frequency may be attributed to the multi-decadal variation of the SST in the North Atlantic Ocean to a large extent (McCabe et al., 2004; Zhang and Delworth, 2006). Additionally, some research indicated that the eastward propagation of wave train can be excited by the warm phase of the AMO throughout the whole Eurasia, and finally increase summer rainfall in Northeast Asia by strengthening the EASM and the southward intrusion of cold air from the north (Si et al., 2020); and it can also increase the Siberian warm-season precipitation by causing anomalous southerly wind, bringing moisture northward (Sun et al., 2015).

However, less research was carried out on the interdecadal and multi-decadal variations over the drylands of the CAD and EAD. It is still unclear which large-scale oceanic oscillation dominates the dry-wet changes in these drylands. For the wetting or drying trend over a long term, the effect from the AMO on the CAD and EAD cannot be ignored. By examining the spatiotemporal characteristics of precipitation over the CAD and EAD at different time scales from 115-year observations, we use atmospheric data to investigate the effects of vertically integrated water-vapor transport on precipitation in different phases of the AMO. Then, we employ the self-calibrating Palmer's drought severity index (scPDSI) dataset to test the reliability of the drought based on precipitation.

2. Data and methods

2.1. Data

The monthly precipitation data used in this study are the Global Precipitation Climatology Centre full data reanalysis version 2020 (GPCC v2020), covering a period from 1891 to 2019 on $0.5^\circ \times 0.5^\circ$ grid

(https://opendata.dwd.de/climate_environment/GPCC/html/fulldat_a-monthly_v2020_doi_download.html). This global land-surface precipitation is based on quality-controlled data from all the stations in the GPCC database for the month, with a maximum number of more than 53,000 stations (Rudolf et al., 2005; Rustemeier et al., 2020; Schneider et al., 2020).

The standardized precipitation index (SPI) and Palmer's drought severity index (PDSI; Palmer, 1965; Agnew, 2000) are commonly used to describe the severity of drought. However, as a superior index to the other drought indices, the scPDSI (van der Schrier et al., 2013; Barichivich et al., 2021) is a better indicator for long-term drought lasting several months to years based on a model considering supply and demand of soil moisture (van der Schrier et al., 2013; Gaire et al., 2019). The dataset of CRU_scPDSI_4.05early used in this paper covers the period from January 1901 to December 2020 at $0.5^\circ \times 0.5^\circ$ resolution (<http://climexp.knmi.nl/select.cgi?id=someone@somewhere&field=scpdsi>).

The monthly AMO index (Enfield et al., 2001) is a detrended time series, defined as regionally weighted mean values of SST anomalies in the North Atlantic from 0° to 70°N . It was calculated from the Kaplan SST dataset at the NOAA Physical Sciences Laboratory, covering the period from 1856 to the present (<https://psl.noaa.gov/data/correlation/amon.us.long.data>). Fig. 1 shows the normalized time series of the AMO index for the period of 1901–2015. The filtered AMO index is obtain by using the ensemble empirical mode decomposition (EEMD) (Wu and Huang, 2009) to remove high-frequency signals and present a clear period of more than 60 years (Zhu et al., 2021a). Specifically, cold AMO phases occurred in 1905–1925 and 1967–1991, while warm phases occurred in 1930–1960 and 1999–2015. These periodic fluctuations of the North Atlantic SST may reside in natural internal variability in the intensity of thermohaline circulation and relevant meridional heat transport in the ocean (Collins and Sinha, 2003; McCabe et al., 2004).

We also use the NOAA-CIRES-DOE Twentieth Century Reanalysis Project version 3 dataset (https://psl.noaa.gov/data/gridded/data.20th_C_ReanV3.html), including monthly pressure at the surface, U/V-component of wind and specific humidity on pressure levels, to calculate the vertically integrated water vapor. The data are on $1^\circ \times 1^\circ$ grid, covering the period from 1836 to 2015. For climate time scales, this dataset has shown a good performance. For example, the multi-decadal averages and long-term time series of the circulation fields correlate well with station-based and other reanalysis products (Slivinski et al., 2019).

2.2. Methods

We use the EEMD (Wu and Huang, 2009) to obtain interannual

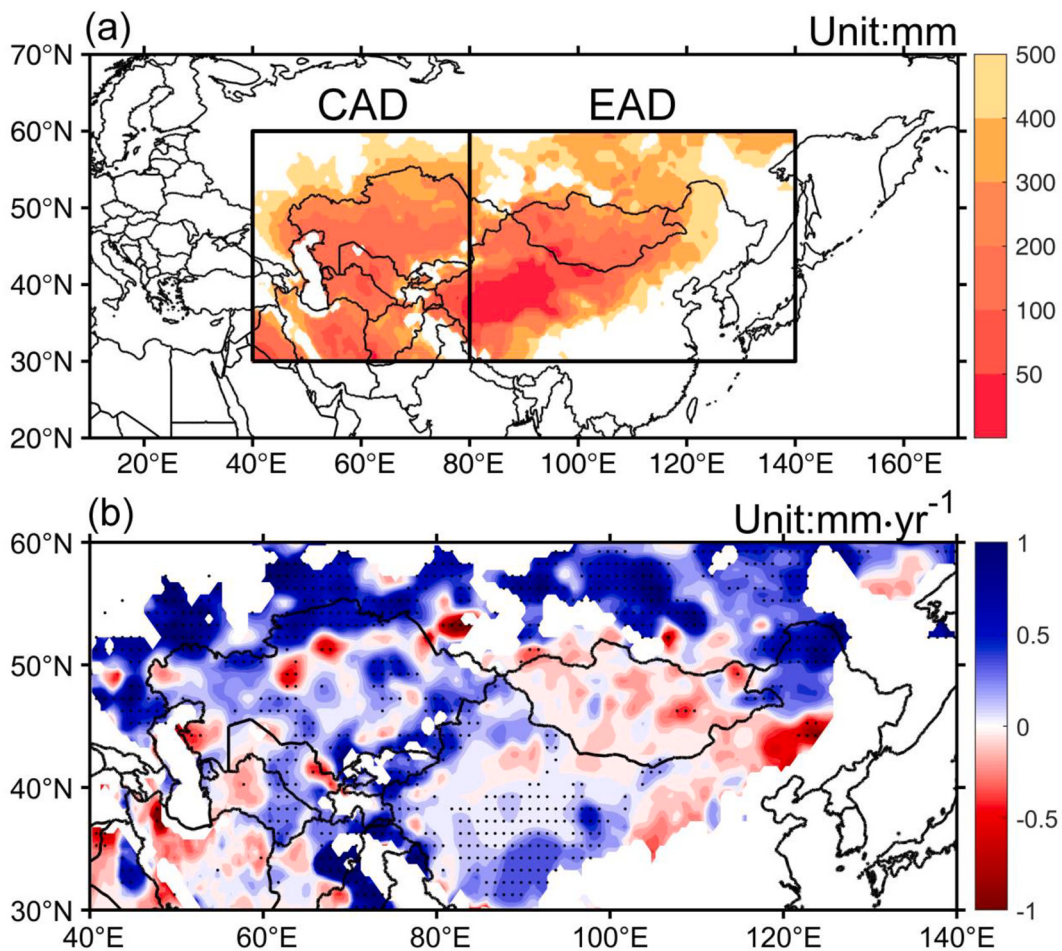


Fig. 2. Spatial distribution of climatological annual mean precipitation (a) and linear trend (b) for precipitation in the CAD and EAD in the period of 1901–2015. Stippling represents the trend significant at the 95% confidence level according to Student's *t*-test.

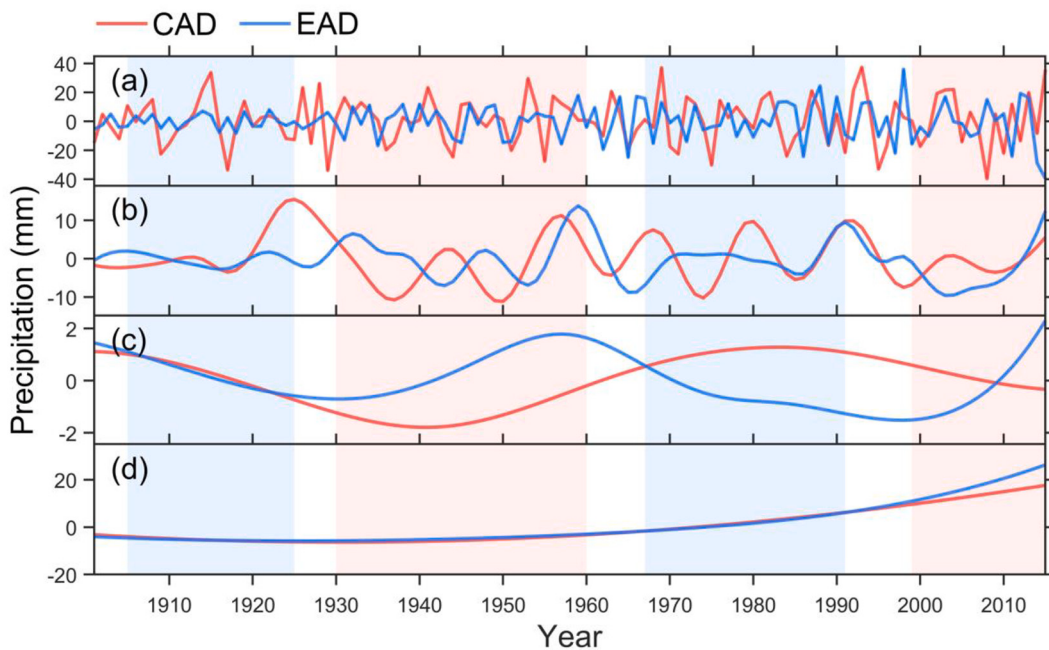


Fig. 3. Interannual variability (a), interdecadal variability (b), multidecadal variability (c), and secular trend (d) of precipitation in the CAD and EAD. Red (blue) shading denotes the positive (negative) period of the AMO. (For interpretation of the references to colour in this figure legend, the reader is referred to the web version of this article.)

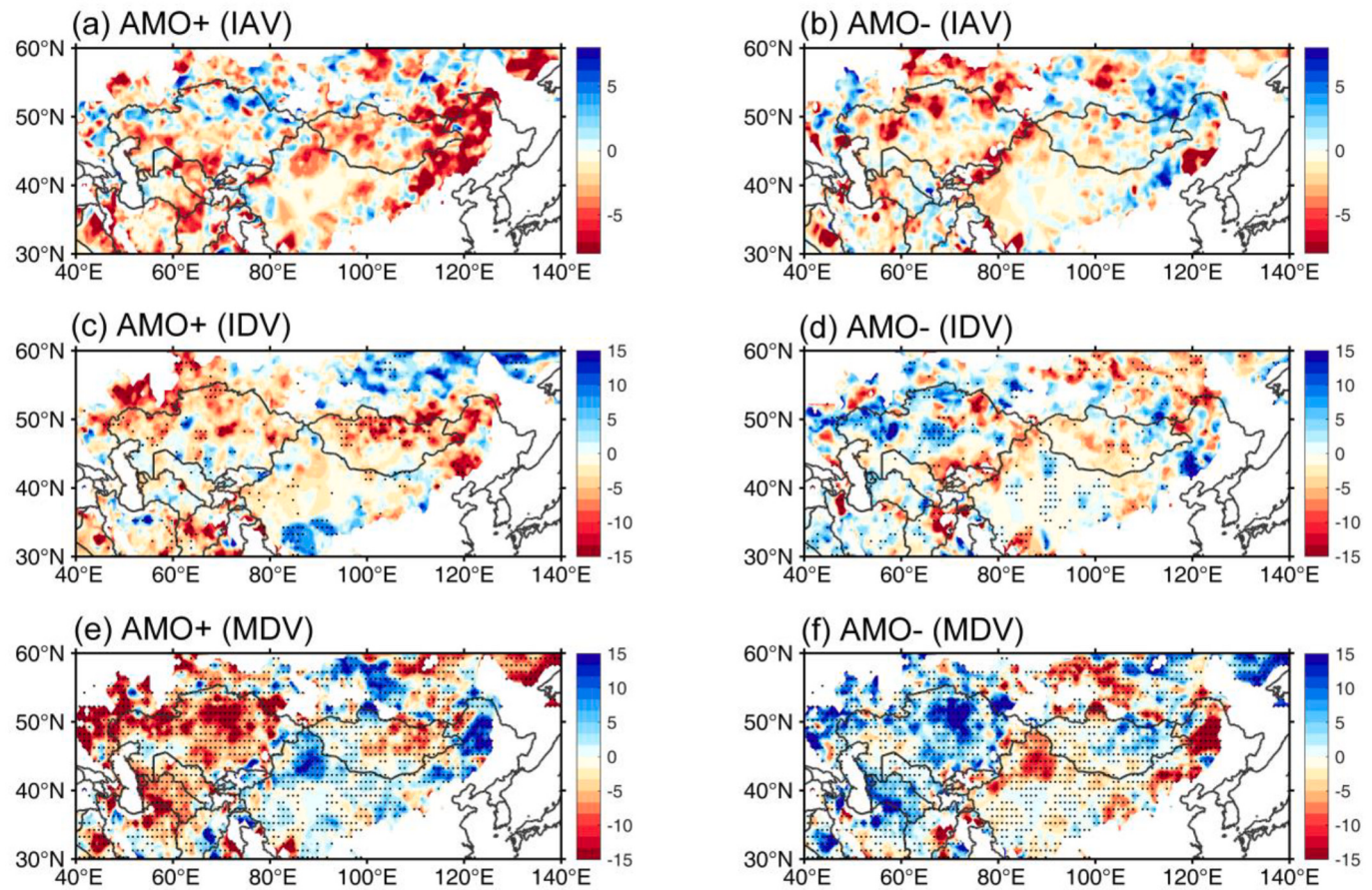


Fig. 4. Left panels: Spatial distributions of precipitation (units: mm) of interannual variability (a), interdecadal variability (c) and multidecadal variability (e) in the warm AMO phase. Right panels: Same as the left ones, except for the cold AMO phase. Stippling indicates significance at the 95% confidence level according to Student's *t*-test.

variability (IAV), interdecadal variability (IDV), multi-decadal variability (MDV), and long-term secular trend (SC) for precipitation in the CAD and EAD. The EEMD is an adaptive method, which is used to decompose non-stationary and nonlinear data into limited intrinsic mode functions (IMFs) with a variety of time scales from short to long periods and a residual named nonlinear trend (Qi et al., 2018).

The empirical orthogonal function (EOF) is a method of feature extraction and dimensionality reduction. As a mainstay of modern data analysis tools, it can produce a composite index that can be used to statistically obtain the weights of individual components and variables (Mainali and Pricope, 2017). The EOF is used for combining diverse correlation indicators to contain as much information as possible from every original dataset. Specifically, when reducing the high dimensionality of the dataset, data patterns can be recognized efficiently by the EOF to minimize the loss of information (Liu and Schisterman, 2004; Kim et al., 2021).

3. Results

3.1. Distribution of precipitation and its trend

Fig. 2a shows the drylands in Central Asia (40° – 80° E, 30° – 60° N) and East Asia (80° – 140° E, 30° – 60° N), where climatological annual mean precipitation is below 500 mm (Huang et al., 2016). The spatial distributions of rainfall in these two regions are distinctive due to clear land-sea and geomorphological contrast. The climate in the CAD is controlled by westerly wind to a great extent, while the eastern part of the EAD, situated in the boundary area of the EASM, is under the monsoon system and westerly wind (Liu et al., 2018). As seen in Fig. 2b, the precipitation

of the CAD and EAD increased during the period of 1901–2015, except in the southwestern part of the CAD, Mongolia and the southeastern part of the EAD (Chen et al., 2011). Furthermore, the southeastern part of the EAD is located in the Asian summer monsoon boundary where the Asian summer monsoon has been broadly weakened, along with rapid decrease in precipitation since the late-1970s (Wang and Ding, 2006; Ding et al., 2008).

3.2. Spatiotemporal variation in precipitation in the warm/cold AMO phase

To understand the variation in precipitation at different time scales in different phases of the AMO, we obtained five IMFs (C1–C5, periods from short to long) and SC component for each region after decomposing the complex signal in weighted average precipitation by using the EEMD method. According to the periods, IAV is the sum of C1 and C2, IDV is the sum of C3 and C4, and MDV is C5 (Fig. 3). The results suggest significant rising trends of annual precipitation in both regions (Fig. 3d), especially since the 1970s, which is in concordance with previous studies. The results also indicate more precipitation over most Asian drylands since the 1980s (Zhang et al., 2021).

Regarding precipitation at different time scales, a phase difference appears between the CAD and EAD, revealing differentiated precipitation changes in these two areas. In particular, the rebuilt IAV (MDV) represents the variation in high-frequency (low-frequency) signals from initial time series. The MDV cycles of the CAD and EAD are approximately 77 a and 58 a, respectively; so it is reasonable that the sum of C4 and C5 represents the MDV of precipitation over these two regions (Fig. 3c). Moreover, the MDV time series of annual precipitation in the

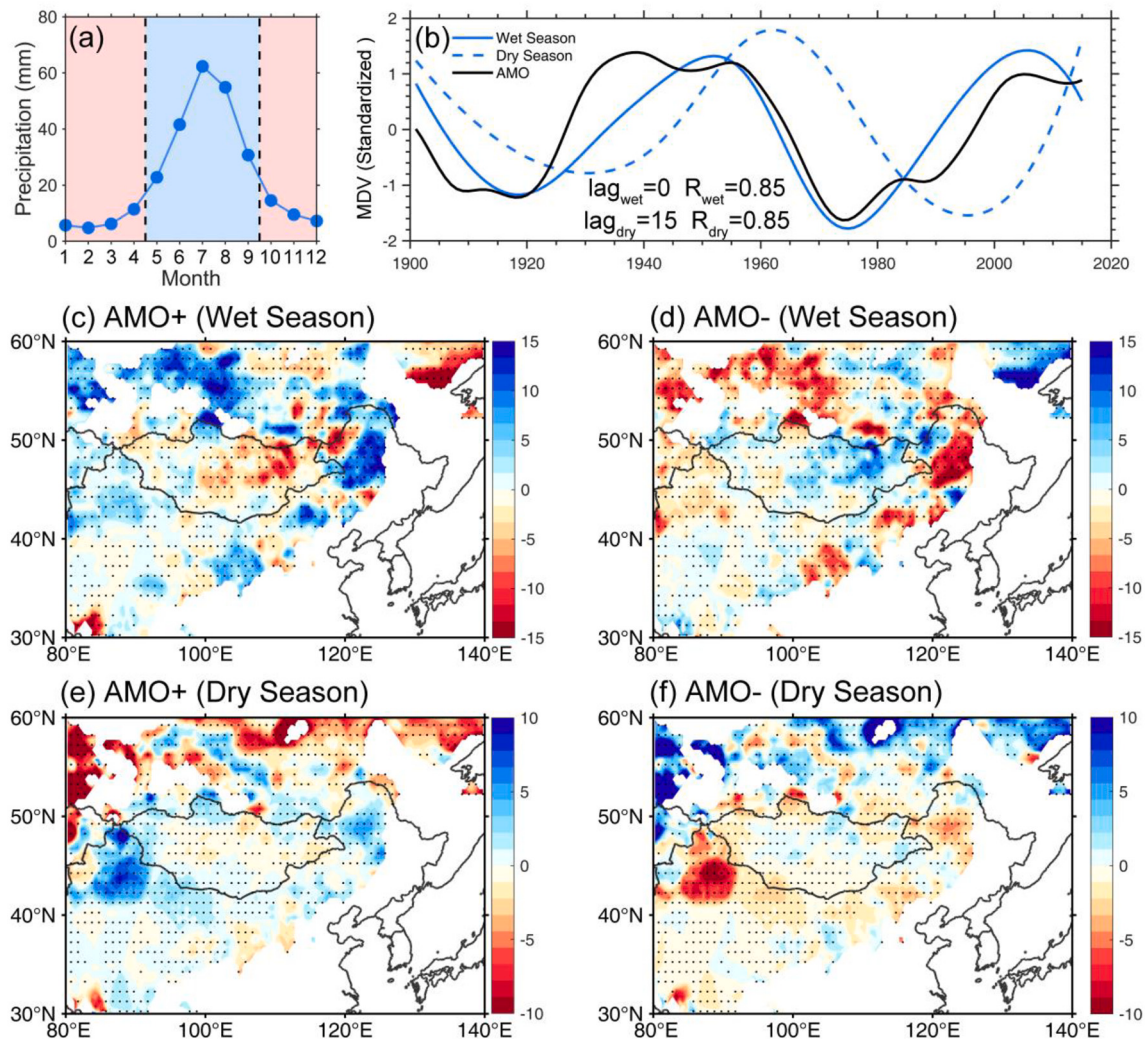


Fig. 5. Monthly variability of precipitation in EAD (a), with red (blue) shading for the wet (dry) season. Lead-lag correlation analysis between standardized MDV index and AMO index in wet and dry seasons in EAD (b). Spatial distributions of the MDV of the precipitation (units: mm) in wet/dry season in the warm AMO phase (c, e) and cold AMO phase (d, f). Stippling indicates significance at the 95% confidence level according to Student's *t*-test. (For interpretation of the references to colour in this figure legend, the reader is referred to the web version of this article.)

CAD exhibits obvious negative (positive) anomalies in the warm (cold) phase of the AMO (Fig. 3c), identifying an out-of-phase relationship.

The EEMD method was also used to decompose the time series of precipitation at each grid point over the CAD and EAD, to delineate precipitation responses at different time scales to the AMO. Spatial distributions of precipitation at different time scales in the warm/cold AMO phase (Fig. 4) show that the MDV of precipitation associated with the AMO should not be ignored. For IAV and IDV (Fig. 4a, b, c, d), there was no obvious symmetrical distribution in most Asian drylands in the warm/cold AMO phase except in some small areas. However, the MDV of precipitation exhibits spatially significant symmetrical responses in different AMO phases, which represents a significant influence of the AMO on the MDV of precipitation. In the warm (cold) AMO phase (Fig. 4e, f), negative (positive) anomalies occupy most of the CAD, representing less-than-normal precipitation at the multi-decadal time scale in the region. In contrast, the EAD shows alternating positive and negative distributions. In particular, there is less (more) precipitation at the multi-decadal time scale in Mongolia and in some areas located in the northeast of the EAD, and more (less) precipitation in the Chinese drylands and the northwest of the EAD during the warm (cold) phase of the AMO.

As the MDV time series of the EAD precipitation do not coincide well

with the AMO transition, we explore the relationship between rainfall and the AMO over the EAD in the wet and dry seasons, respectively, for the precipitation in the EAD has remarkable seasonal cycle (Fig. 5a). The precipitation in the EAD is concentrated from May to September (wet season); and less precipitation occurred from October to the following April (dry season; Fig. 5a). The lead-lag correlation between the AMO and MDV of precipitation in the CAD and EAD is also analyzed (Fig. 5b). In the dry season, the AMO leads the MDV of precipitation by 15 years ($\text{lag} = 15, R = 0.85, p < 0.01$). However, the MDV of precipitation in the wet season has significant simultaneous correlation with the AMO ($\text{lag} = 0, R = 0.85, p < 0.01$), showing a synchronous change.

This synchronous change can be manifested in the spatial distribution of the MDV of wet season in different AMO phases. During the warm (cold) AMO phase, more areas in the EAD experience above-normal (below-normal) precipitation in the wet season in comparison with the map of the composite MDV of annual precipitation (Figs. 4e, f, 5c, d). As seen in the spatial distribution of precipitation on the multi-decadal time scale in the dry season (Fig. 5e and f), negative anomalies are mainly distributed in the north of the EAD in the warm AMO phase (Fig. 5e), while positive anomalies occupy the south part of the EAD (most regions in Mongolia and China). Symmetrical response of the MDV of precipitation in the dry season can be found in the AMO cold phase (Fig. 5f).

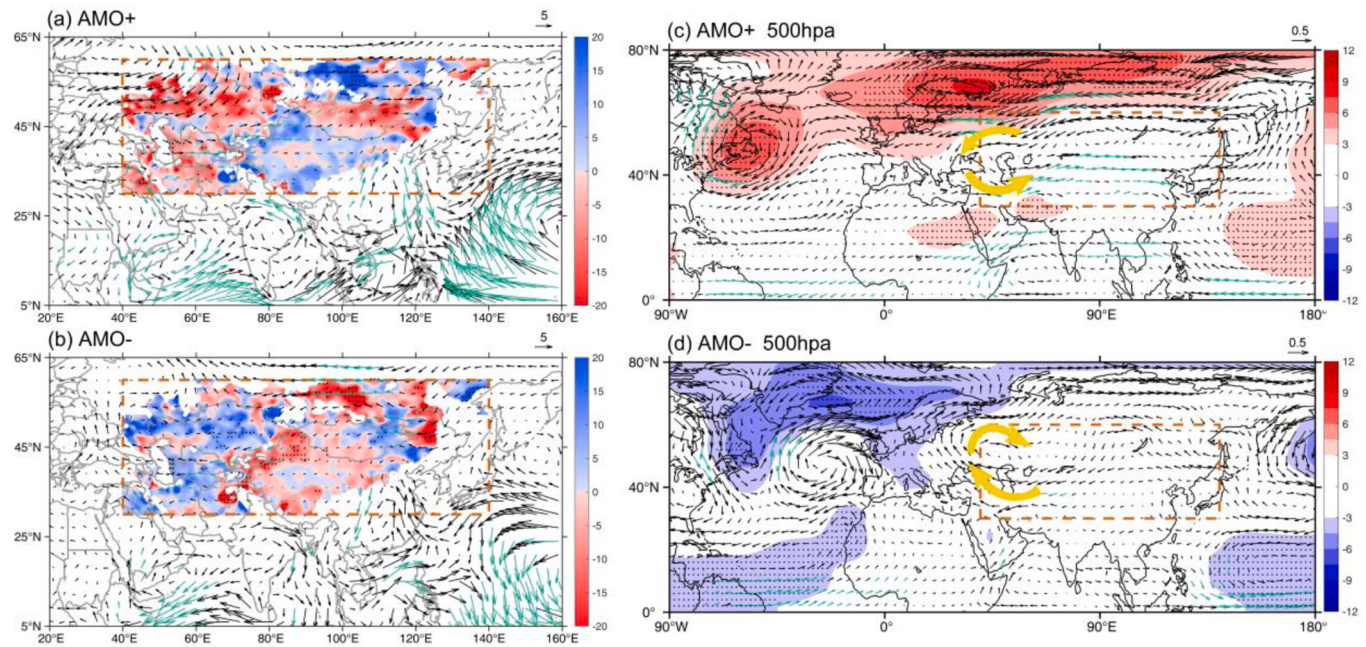


Fig. 6. Composite vertically integrated water-vapor flux (arrow; 1000–300 hPa; units: $\text{kg} \cdot \text{m}^{-1} \cdot \text{s}^{-1}$) and precipitation anomalies (contour; units: mm) in the warm (a) and cold (b) AMO phases. Composite geopotential height (contour; units: m) and wind (arrow) at 500 hPa in the warm (c) and cold (d) AMO phases. Stippling indicates significance at the 95% confidence level of *t*-test for precipitation anomalies or geopotential height field; Green vector indicates significance at the 95% confidence level. (For interpretation of the references to colour in this figure legend, the reader is referred to the web version of this article.)

Given that the precipitation on the multi-decadal time scale of the wet season correlates well with the AMO index in the EAD (Fig. 5b), and a negative correlation between the multi-decadal precipitation and the AMO index in the CAD (Figs. 4e, f, 5c, d), a more stable opposite relationship of precipitation of the CAD and EAD can be established in each phase of the AMO.

3.3. Influence of the AMO on water-vapor transport

To understand the relationship between the AMO and precipitation, we analyzed the regional water-vapor transport for precipitation over Asian drylands. Fig. 6 shows the composite vertically integrated water-vapor flux and precipitation anomalies in the warm/cold AMO phase. In the warm phase, most CAD regions have less precipitation, while the precipitation over most EAD regions is above normal except for some regions, e.g., Mongolia. The dry-wet pattern is the opposite in the cold AMO phase (Kamae et al., 2017; Zhu et al., 2021a).

Such precipitation change is closely associated with water-vapor transport. In the positive phase of the AMO (Fig. 6a), enhanced north-eastward moisture transport occurs over the Arabian Sea, Bay of Bengal and western Pacific. Furthermore, anomalous north-to-south water-vapor flux is favorable for less precipitation. Anomalous southward moisture transport over the Arabian Peninsula significantly contributes to the decreased atmospheric precipitable water in the south of the CAD during the warm AMO phase, reinforcing the precipitation anomalies. Kazakhstan, the main body of the CAD (Dilinuer et al., 2021), exhibits an obvious negative anomaly of precipitation as a result of the weakened mid-latitude water-vapor transport from the west in the warm AMO phase. An opposite pattern of composited precipitation and water-vapor flux is found in the cold AMO phase (Fig. 6b).

The circulation anomalies composite for the warm AMO phase at 500 hPa (Fig. 6c) indicates that an anomalous cyclonic circulation occurred over the mid-upper level of the CAD accompanied by subsidence, which is unfavorable to the formation of precipitation. This anomalous mid-upper level convergence agrees well with the situation in which precipitation is less than normal over the CAD in the warm

AMO phase. In contrast, in the cold phase of the AMO, there is an anticyclonic circulation anomaly over the CAD, as the result of the ascending motion from the lower troposphere, which brings more precipitation.

For most of the EAD region (Fig. 6a), the enhanced EASM results in above-normal precipitation; and for northern Mongolia, moisture transport from the west is stronger than normal, which may be due to the enhancement of the westerly wind over this region during the warm phase of the AMO (Si et al., 2020). In tandem with the influence of the enhanced EASM, more precipitation in Chinese drylands is simultaneously influenced by anomalous southwesterly moisture flux associated with strengthened water-vapor transport over the Indian Ocean; however, significant negative precipitable water accompanied by anomalous northward moisture transport from the southeastern coastal region of China covers most Mongolian drylands, while the opposite condition occurs in the cold phase of the AMO (Fig. 6b).

By comparing Fig. 6a and b, it is apparent that the precipitation over the CAD and EAD change almost oppositely in each phase of the AMO. This significant contrast of precipitation anomalies is affected by changes in the Indian summer monsoon (ISM) and EASM. A positive AMO causes warming of the North Pacific via air-sea interaction, subsequently inducing easterly anomalies along the equatorial Pacific and then enhancing the ISM (Goswami et al., 2006; Luo et al., 2018). There is also a positive correlation between the AMO and EASM. Previous studies showed that the cooling of the North Atlantic leads to anomalous convergent winds in the western tropical Pacific, which weakens the EASM (Lu et al., 2006; Yu et al., 2009), causing less precipitation in the EAD. During the warm AMO phase, the weakened westerly wind contributes to less precipitation in the CAD; thus, such opposite distribution characteristics of precipitation anomalies over the CAD and EAD are the result of the variations in the monsoon system and westerly intensity under the influence of the AMO.

3.4. Response of drought frequency to the AMO

Considering the strong influence of the AMO on the MDV of

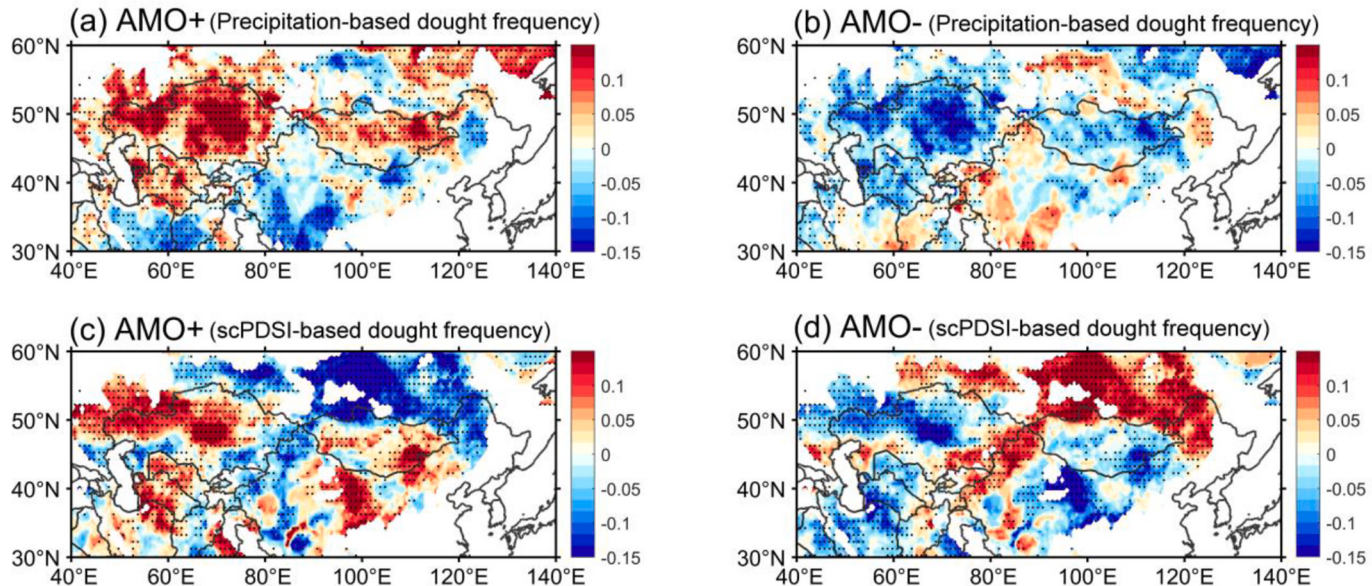


Fig. 7. Composite drought frequency by using precipitation in warm (a) and cold (b) AMO phases, and by using the scPDSI in warm (c) and cold (d) AMO phases. Stippling denotes the region with statistical significance at the 95% confidence level based on Student's *t*-test.

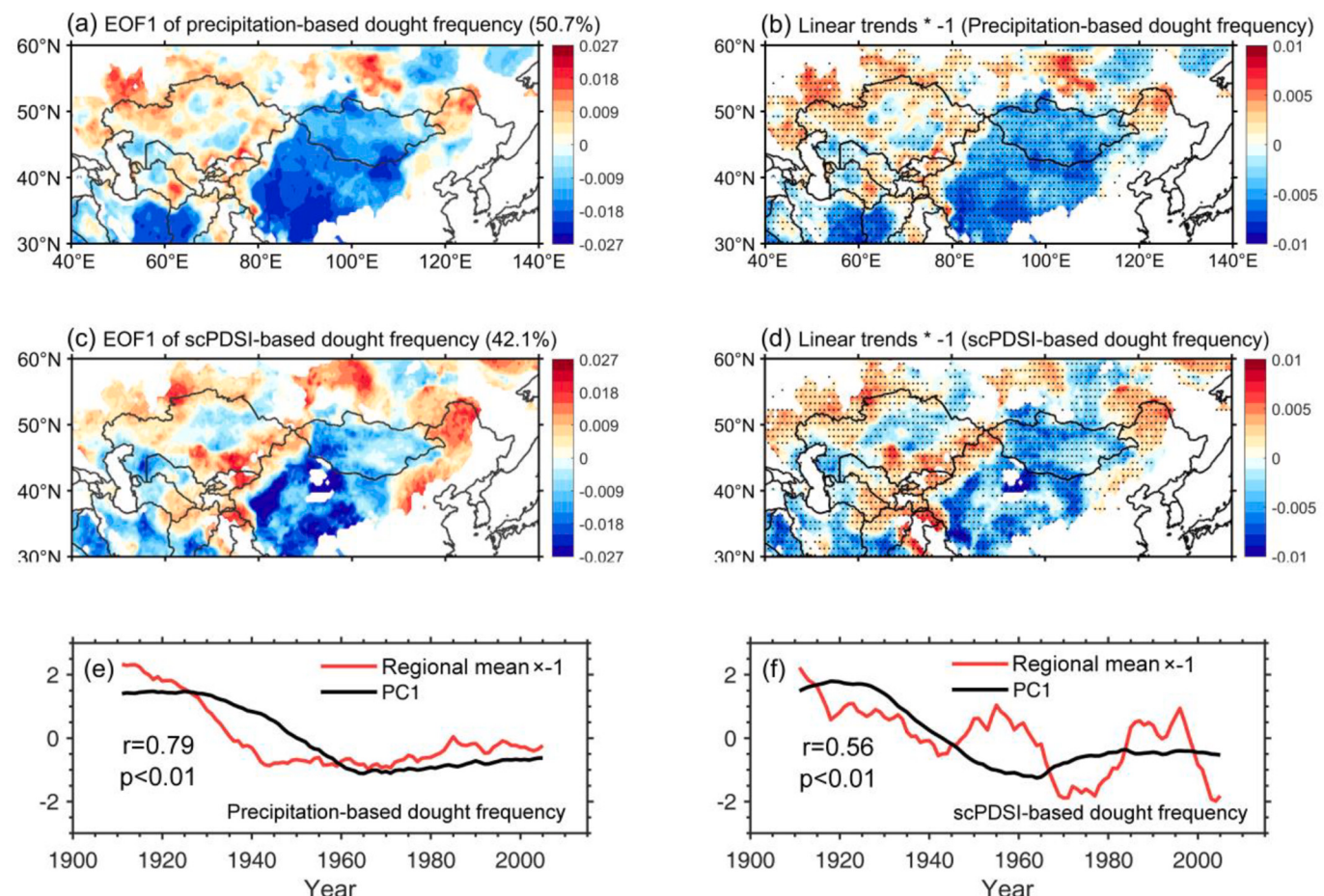


Fig. 8. Spatial pattern of EOF1 of 20-year moving drought frequency based on precipitation (a) and scPDSI (c). Map of the linear trend (multiplied by -1 , units: yr^{-1}) for 20-year moving drought frequency based on precipitation (b) and scPDSI (d). Stippling indicates significance at the 95% confidence level. The standardized PC1 time series of the 20-year moving drought frequency based on precipitation (e) and scPDSI (f) compared with each corresponding standardized area-averaged time series (multiplied by -1).

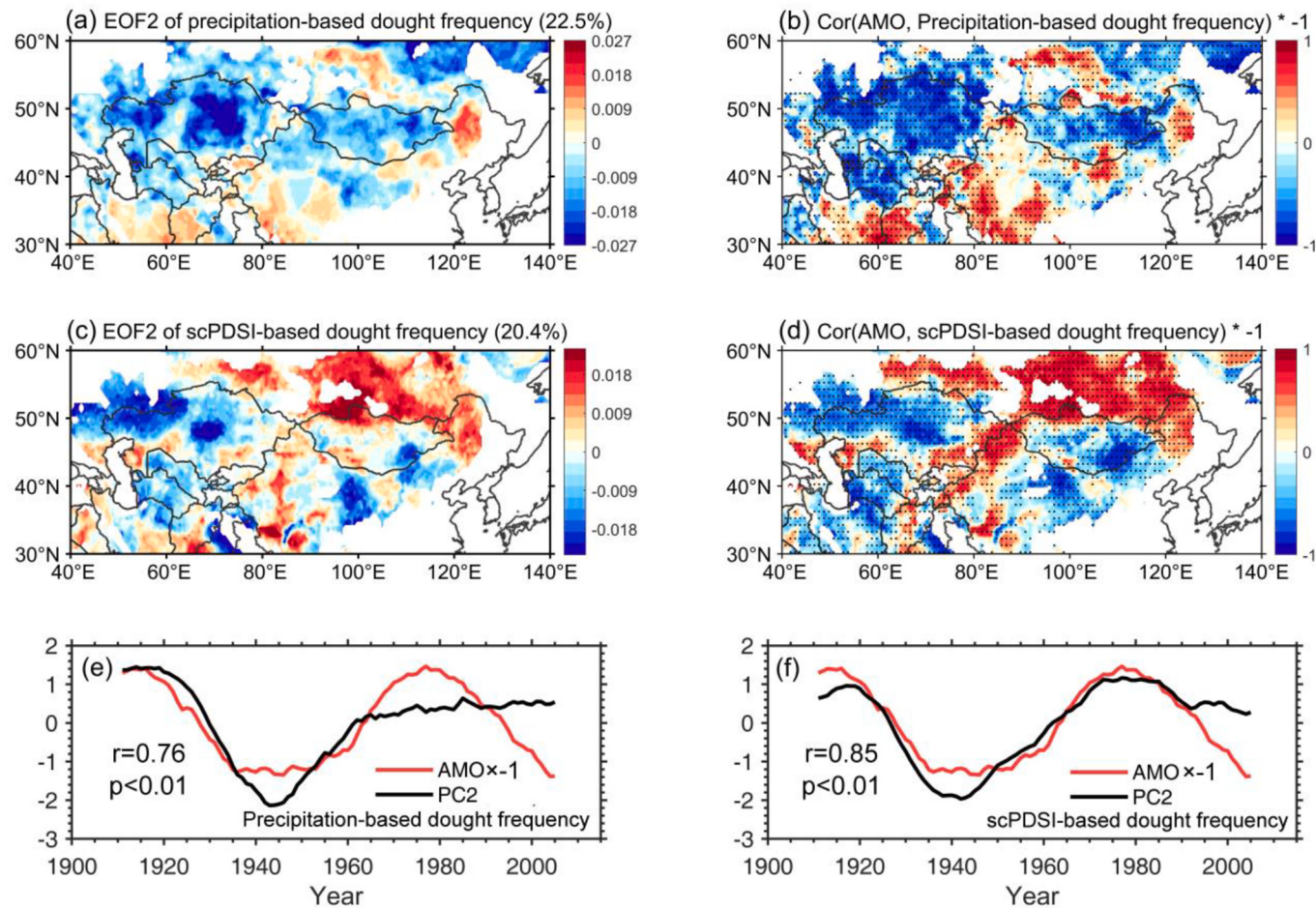


Fig. 9. Spatial pattern of EOF2 of the 20-year moving drought frequency based on precipitation (a) and scPDSI (c). Map of correlations (multiplied by -1) between the 20-year moving annual AMO and 20-year moving drought frequency based on precipitation (b) and scPDSI (d). Stippling indicates significance at the 95% confidence level. The standardized PC2 time series of the 20-year moving drought frequency based on precipitation (e) and scPDSI (f) compared with the standardized 20-year moving AMO (multiplied by -1).

precipitation and the magnitude of drought frequency analysis for evaluating extreme drought, especially in drylands (Li et al., 2021), we analyzed the relationship of the AMO and drought frequency at the multi-decadal time scale. A drought year is defined as the year with precipitation in the lowest quartile (25%) of the 115 years or the scPDSI below -1.0 . Then, we used 20-year moving window to compute the number of drought years, which were assigned to the center of the window (McCabe et al., 2004); and we compared the time series of drought frequency on the multi decadal time scale.

As shown in Fig. 7, the composite drought frequencies based on precipitation and scPDSI present a spatially symmetric relationship during different AMO phases, identifying that the AMO has a significant impact on the drought frequency. The pattern of composite drought frequency based on precipitation has a good agreement with that based on the scPDSI, except in the northeastern part of the EAD. These patterns consistently indicate an opposite relationship of drought frequency between the CAD and EAD, which is consistent with the precipitation variation in most regions. The positive-value area is mainly distributed in the central and northern parts of the EAD and Mongolia, representing more drought events in the warm AMO phase (Fig. 7a and c). The opposite pattern of drought frequency variation is found in the negative AMO phase (Fig. 7b and d).

To identify the principal modes of variability in drought frequency, we used EOF analysis. Then, we compared the spatial patterns of the first two EOF models with the spatial distributions of the linear trend of drought frequency; and we studied the correlations between the 20-year

moving average AMO and 20-year moving drought frequencies, to better understand how the AMO is associated to the temporal and spatial variation of drought in the CAD and EAD. The first two EOF modes (EOF1 and EOF2) for the multi-decadal variability of the precipitation-based (scPDSI-based) drought frequency account for 50.7% and 22.5% (42.1% and 20.4%) of the total variance.

The spatial pattern of EOF1 and the spatial distribution of the linear trend of drought frequency (Fig. 8) are highly similar for precipitation-based and scPDSI-based drought frequencies. The correlation between EOF1 and the spatial distribution of the linear trend of drought frequency based on precipitation (scPDSI) is 0.97 (0.88); both are significant at the 99th percentile. Although the correlation between the two time series in Fig. 8f is 0.56 ($p < 0.01$) for the temperature plays an important role in the change of the scPDSI-based drought frequency (Fig. 8f), the first principal component (PC1) of EOF1 on the precipitation-based drought frequency correlates well with its area-averaged time series ($r = 0.79$, $p < 0.01$; Fig. 8e).

Hence, we use EOF1 of the drought frequency to represent its long-term linear trend. Because the linear trend was multiplied by -1 to compare with EOF1 easily, regions with negative values have an increasing trend in drought frequency, and regions with positive values have a decreasing trend in drought frequency (Fig. 8a and c). Geographically, Mongolia, Northwest China drylands, central Kazakhstan, and the southwestern part of the CAD experience an increasing tendency of drought, while the Northeast China drylands, the northwestern part of the CAD, and the border region of China and

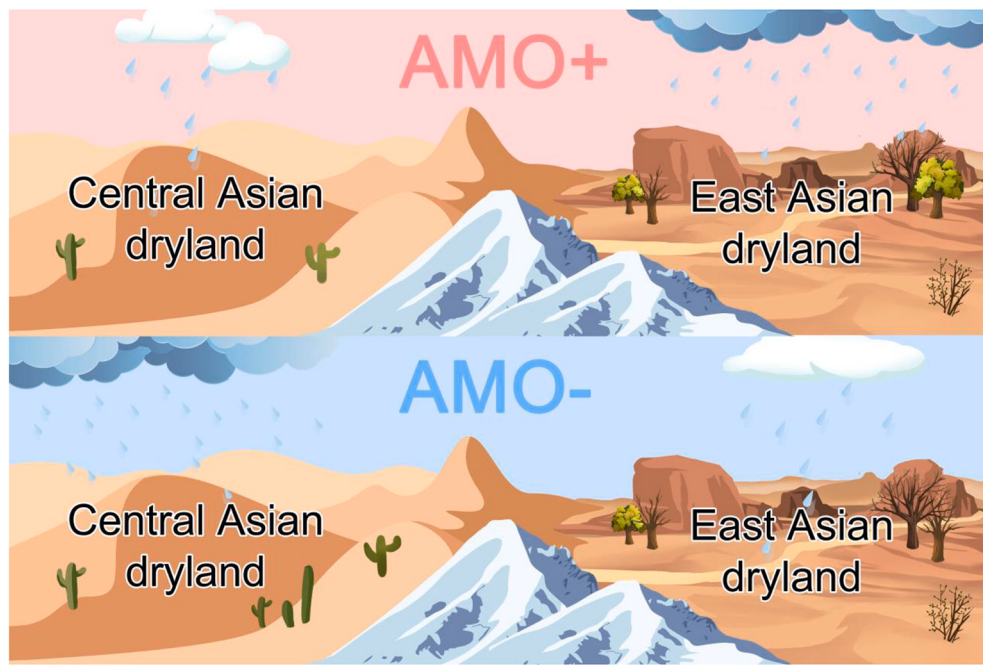


Fig. 10. Different dry/wet conditions in CAD and EAD during the warm/cold AMO phase.

Kazakhstan see a decline in drought frequency.

Fig. 9a, b, c, and d indicate that correlations between the 20-year moving drought frequency and 20-year moving averaged AMO resemble the spatial pattern of EOF2 regardless using precipitation-based or scPDSI-based drought frequency, in spite of small regional differences in the correlation patterns. The correlations between EOF2 and the correlation maps of drought frequency based on precipitation and scPDSI are 0.82 and 0.86, respectively, both being significant at the 99% confidence level. A strong correlation of the two time series can also be represented by the PC2 and the AMO for either precipitation-based or scPDSI-based drought frequency (0.76 and 0.85; Fig. 9e and f). Therefore, EOF2 of the drought frequency is dominated by the AMO. The AMO correlations indicate positive values for Mongolia and most of the CAD, and negative values for the northern part of the EAD since the correlation coefficients were multiplied by -1 (Fig. 9b and d). EOF2 explains 22% (20%) of the variance in drought frequency based on precipitation (scPDSI).

4. Discussion and conclusions

We examined long-term variation in the annual precipitation of the CAD and EAD on different time scales since 1901. We found opposite variation patterns of precipitation on the multi-decadal time scale between the CAD and EAD in each AMO phase (Fig. 10), spatially and temporally, especially in the wet season. The precipitation over the CAD and EAD were dominated by the westerly and monsoons (the EASM and ISM), respectively. The contrast of precipitation anomalies between the two regions was the result of enhanced monsoons and weakened westerly associated with the positive AMO phase, which brought more moisture to the EAD and less to the CAD; and the opposite pattern occurred in the negative AMO phase.

The AMO exerted a considerable influence on multi-decadal drought changes. According to the EOF results on precipitation-based and scPDSI-based drought frequency, more than 20% spatiotemporal variance in drought on the multi-decadal time scale was due to the AMO. Meanwhile, the AMO-induced dry/wet patterns were consistent with the results of drought reconstructed by tree rings in some local areas in published studies, such as the Tianshan Mountains (in Northwest China; Wang et al., 2021), the northern Daxing'an Mountains (on the

northernmost border of China; Zhu et al., 2021b), the Dzungarian Alatau (between the Zhetyssu region of Kazakhstan and the Dzungaria region of China; Zhang et al., 2017), and Mongolia (Pederson et al., 2001). For example, a prominent drought event in 1945 (in the warm AMO phase) was detected in the central Tianshan Mountains and Mongolia. In addition, Zhang et al. (2017) found that in the Dzungarian Alatau, two abrupt (wet-dry, dry-wet) changes occurred in 1950 and 1974 (the year in cold AMO phase and the year in warm AMO phase, respectively); they also pointed out possible links between the changes of the PDSI and the large-scale oscillations in the climate system.

Our results here strongly support this hypothesis in Zhang et al. (2017) and confirmed the indispensable role of the AMO in drought variability. Considering the impact of the AMO on the drought reconstructed by tree rings, a good correlation between the AMO and moisture-sensitive tree growth on long time scales can be established, which can help us understand the response of the ecology to the warm/cold AMO phase in the CAD and EAD. If the current warm phase of the AMO persists, the northern EAD will experience dry condition, and the CAD and Mongolia will be in wet condition.

CRediT authorship contribution statement

Shuyang Guo: Conceptualization, Methodology, Data curation, Visualization, Writing – original draft, Software. **Xiaodan Guan:** Conceptualization, Supervision, Writing – review & editing, Funding acquisition, Investigation. **Linlin Gao:** Validation, Investigation. **Wen Sun:** Visualization, Writing – review & editing. **Chenyu Cao:** Writing – review & editing. **Yongli He:** Writing – review & editing.

Declaration of Competing Interest

The authors declare that they have no known competing financial interests or personal relationships that could have appeared to influence the work reported in this paper.

Acknowledgments

This work is supported by the National Science Foundation of China (42041004 and 41991231), the Strategic Priority Research Program of

the Chinese Academy of Sciences (No. XDA2006010301), the “Innovation Star” Project for Outstanding Postgraduates of Gansu Province (2021CXZX-102, 2021CXZX-103), and the Central Universities (lzujbky-2019-kb30).

References

- Agnew, C., 2000. Using the SPI to identify drought. *Drought Netw. News* 12 (1), 6–12.
- Aizen, E.M., Aizen, V.B., Melack, J.M., Nakamura, T., Ohta, T., 2001. Precipitation and atmospheric circulation patterns at mid-latitudes of Asia. *Int. J. Climatol.* 21 (5), 535–556. <https://doi.org/10.1002/joc.626>.
- Barichivich, J., Osborn, T.J., Harris, I., van der Schrier, G., Jones, P.D., 2021. Monitoring global drought using the self-calibrating Palmer Drought Severity Index [in “State of the Climate in 2020” eds. Dunn RHJ, Aldred F, Gobron N, Miller JB & Willett KM]. *Bull. Am. Meteorol. Soc.* 102, S68–S70. <https://doi.org/10.1175/BAMS-D-21-0098.1>.
- Chen, F., Huang, W., 2017. Multi-scale climate variations in the arid Central Asia. *Adv. Clim. Chang. Res.* 8 (1), 1–2. <https://doi.org/10.1016/j.accre.2017.02.002>.
- Chen, F., Huang, W., Jin, L., Chen, J., Wang, J., 2011. Spatiotemporal precipitation variations in the arid Central Asia in the context of global warming. *Sci. China Earth Sci.* 54 (12), 1812–1821. <https://doi.org/10.1007/s11430-011-4333-8>.
- Chen, W., Lee, J., Lu, R., Dong, B., Ha, K., 2015. Intensified impact of tropical Atlantic SST on the western North Pacific summer climate under a weakened Atlantic thermohaline circulation. *Clim. Dyn.* 45 (7), 2033–2046. <https://doi.org/10.1007/s00382-014-2454-4>.
- Collins, M., Sinha, B., 2003. Predictability of decadal variations in the thermohaline circulation and climate. *Geophys. Res. Lett.* 30 (6) <https://doi.org/10.1029/2002GL016504>.
- Dilinuer, T., Yao, J., Chen, J., Mao, W., Yang, L., Yeernaer, H., Chen, Y., 2021. Regional drying and wetting trends over Central Asia based on Köppen climate classification in 1961–2015. *Adv. Clim. Chang. Res.* <https://doi.org/10.1016/j.accre.2021.05.004>.
- Ding, Y., Wang, Z., Sun, Y., 2008. Inter-decadal variation of the summer precipitation in East China and its association with decreasing Asian summer monsoon. Part I: Observed evidences. *Int. J. Climatol.* 28 (9), 1139–1161. <https://doi.org/10.1002/joc.1615>.
- Enfield, D.B., Mestas-Nuñez, A.M., Trimble, P.J., 2001. The Atlantic multidecadal oscillation and its relation to rainfall and river flows in the continental U.S. *Geophys. Res. Lett.* 28 (10), 2077–2080. <https://doi.org/10.1029/2000GL012745>.
- Gaire, N.P., Dhakal, Y.R., Shah, S.K., Fan, Z., Bräuning, A., Thapa, U.K., Bhandari, S., Aryal, S., Bhuju, D.R., 2019. Drought (scPDSI) reconstruction of trans-Himalayan region of central Himalaya using *Pinus wallichiana* tree-rings. *Palaeogeogr. Palaeoclimatol. Palaeoecol.* 514, 251–264. <https://doi.org/10.1016/j.palaeo.2018.10.026>.
- Goswami, B.N., Madhusoodanan, M.S., Neema, C.P., Sengupta, D., 2006. A physical mechanism for North Atlantic SST influence on the Indian summer monsoon. *Geophys. Res. Lett.* 33 (2), L02706. <https://doi.org/10.1029/2005gl024803>.
- Guan, X., Huang, J., Guo, R., Yu, H., Lin, P., Zhangm, Y., 2015. Role of radiatively forced temperature changes in enhanced semi-arid warming in the cold season over East Asia. *Atmos. Chem. Phys.* 15 (23), 13777–13786.
- Guan, X., Huang, J., Zhang, Y., Xie, Y., Liu, J., 2016. The relationship between anthropogenic dust and population over globalsemi-arid regions. *Atmos. Chem. Phys.* 16 (8) <https://doi.org/10.5194/acp-16-5159-2016>.
- Guan, X., Ma, J., Huang, J., Huang, R., Zhang, L., Ma, Z., 2019. Impact of oceans on climate change in drylands. *Sci. China Earth Sci.* 62 (6), 891–908. <https://doi.org/10.1007/s11430-018-9317-8>.
- Guan, X., Zhu, K., Huang, X., Zeng, X., Zhang, L., He, Y., 2021. Precipitation changes in semi-arid regions in East Asia under global warming. *Front. Earth Sci.* <https://doi.org/10.3389/feart.2021.762348>.
- Guo, R., Guan, X., He, Y., Gan, Z., Jin, H., 2018. Different roles of dynamic and thermodynamic effects in enhanced semi-arid warming. *Int. J. Climatol.* 38 (1), 13–22. <https://doi.org/10.1002/joc.5155>.
- Hua, L.J., Ma, Z.G., 2009. The evolution of dry and wet periods in Asia and North America and its relationship with SSTA. *Chin. J. Geophys.* 52 (05), 1184–1196.
- Huang, J., Ji, M., Xie, Y., Wang, S., He, Y., Ran, J., 2016. Global semi-arid climate change over last 60 years. *Clim. Dyn.* 46 (3–4), 1131–1150. <https://doi.org/10.1007/s00382-015-263-8>.
- Jeff, R.K., Chris, K.F., Adam, A.S., 2006. Climate impacts of the Atlantic Multidecadal Oscillation. *Geophys. Res. Lett.* 33 (17), L17706. <https://doi.org/10.1029/2006GL026242>.
- Joshi, M.K., Ha, K., 2019. Fidelity of CMIP5-simulated teleconnection between Atlantic multidecadal oscillation and Indian summer monsoon rainfall. *Clim. Dyn.* 52 (7), 4157–4176. <https://doi.org/10.1007/s00382-018-4376-z>.
- Joshi, M.K., Pandey, A.C., 2011. Trend and spectral analysis of rainfall over India during 1901–2000. *J. Geophys. Res. Atmos.* 116 (D6), D06104. <https://doi.org/10.1029/2010jd014966>.
- Kamae, Y., Li, X., Xie, S., Ueda, H., 2017. Atlantic effects on recent decadal trends in global monsoon. *Clim. Dyn.* 49 (9–10), 3443–3455. <https://doi.org/10.1007/s00382-017-3522-3>.
- Kim, J., Yu, J., Ryu, J., Lee, J., Kim, T., 2021. Assessment of regional drought vulnerability and risk using principal component analysis and a Gaussian mixture model. *Nat. Hazards.* <https://doi.org/10.1007/S11069-021-04854-Y>.
- Li, S.L., Gary, T.B., 2007. Influence of the Atlantic Multidecadal Oscillation on the winter climate of East China. *Adv. Atmos. Sci.* 24 (1), 126–135. <https://doi.org/10.1007/s00376-007-0126-6>.
- Li, Y., Lu, H., Yang, K., Wang, W., Tang, Q., Khem, S., Yang, F., Huang, Y., 2021. Meteorological and hydrological droughts in Mekong River Basin and surrounding areas under climate change. *J. Hydrol. Reg. Stud.* 36 <https://doi.org/10.1016/j.ejrh.2021.100873>.
- Liu, A., Schisterman, E.F., 2004. Principal component analysis. In: Chow, S.-C. (Ed.), *Encyclopedia of Biopharmaceutical Statistics*. CPC Press, New York, pp. 1796–1801.
- Liu, C., Xia, J., 2004. Water problems and hydrological research in the Yellow River and the Huai and Hai River basins of China. *Hydrol. Process.* 18 (12), 2197–2210. <https://doi.org/10.1002/hyp.5524>.
- Liu, Y., Wu, C., Jia, R., Huang, J., 2018. An overview of the influence of atmospheric circulation on the climate in arid and semi-arid region of Central and East Asia. *Sci. China Earth Sci.* 61 (9), 1183–1194. <https://doi.org/10.1007/s11430-017-9202-1>.
- Lu, R., Dong, B., Ding, H., 2006. Impact of the Atlantic Multidecadal Oscillation on the Asian summer monsoon. *Geophys. Res. Lett.* 33, L24701. <https://doi.org/10.1029/2006GL027655>.
- Luo, F., Li, S., Gao, Y., Svendsen, L., Furevik, T., Keenlyside, N., 2018. The connection between the Atlantic multidecadal oscillation and the Indian summer monsoon in CMIP5 models. *Environ. Res. Lett.* 13, 094020 <https://doi.org/10.1088/1748-9326/aade11>.
- Lyu, K.W., Yu, J.Y., Paek, H., 2017. The influences of the atlantic multidecadal oscillation on the mean strength of the North Pacific subtropical high during boreal winter. *J. Clim.* 30 (1), 411–426. <https://doi.org/10.1175/JCLI-D-16-0525.1>.
- Mainali, J., Principe, N.G., 2017. High-resolution spatial assessment of population vulnerability to climate change in Nepal. *Appl. Geogr.* 82, 66–82. <https://doi.org/10.1016/j.apgeog.2017.03.008>.
- McCabe, G.J., Palecki, M.A., Betancourt, J.L., 2004. Pacific and Atlantic Ocean influences on multidecadal drought frequency in the United States. *Proc. Natl. Acad. Sci.* 101 (12), 4136–4141. <https://doi.org/10.1073/pnas.0306738101>.
- Mohino, E., Janicot, S., Bader, J., 2011. Sahel rainfall and decadal to multi-decadal sea surface temperature variability. *Clim. Dyn.* 37 (3–4), 419–440. <https://doi.org/10.1007/s00382-010-0867-2>.
- Palmer, W.C., 1965. Meteorological drought. In: *Weather Bureau Research Paper 45*. United States Department of Commerce, Washington DC.
- Pederson, N., Jacoby, G.C., D'Arrigo, R.D., Cook, E.R., Buckley, B.M., Dugarjav, C., Mijiddorj, R., 2001. Hydrometeorological reconstructions for northeastern Mongolia derived from tree rings: AD 1651–1995. *J. Clim.* 14, 872–881.
- Qi, Y., Yan, Z., Qian, C., Sun, Y., 2018. Near-term projections of global and regional land mean temperature changes considering both the secular trend and multidecadal variability. *J. Meteorol. Res.* 32 (03), 337–350. <https://doi.org/10.1007/s13351-018-17136-4>.
- Reed, S.C., Coe, K.K., Sparks, J.P., Housman, D.C., Zelikova, T.J., Belnap, J., 2012. Changes to dryland rainfall result in rapid moss mortality and altered soil fertility. *Nat. Clim. Chang.* 2 (10), 752–755. <https://doi.org/10.1038/nclimate1596>.
- Rudolf, B., Beck, C., Grieser, J., Schneider, U., 2005. *Global Precipitation Analysis Products*. Global Precipitation Climatology Centre (GPCC), DWD, Internet Publication, pp. 1–8.
- Rustemeier, E., Becker, A., Finger, P., Schneider, U., Ziese, M., 2020. GPCC Climatology Version 2020 at 0.5°: Monthly Land-Surface Precipitation Climatology for Every Month and the Total Year from Rain-Gauges Built on GTS-Based and Historical Data. https://doi.org/10.5676/DWD_GPCC/CLIM_M_V2020_050.
- Schneider, U., Becker, A., Finger, P., Rustemeier, Elke, Ziese, M., 2020. GPCC Full Data Monthly Product Version 2020 at 0.5°: Monthly Land-Surface Precipitation from Rain-Gauges Built on GTS-Based and Historical Data. https://doi.org/10.5676/DWD_GPCC/FD_M_V2020_050.
- Schwinning, S., Sala, O.E., Loik, M.E., Ehleringer, J.R., 2004. Thresholds, memory, and seasonality: understanding pulse dynamics in arid/semi-arid ecosystems. *Oecologia* 141 (2), 191–193. <https://doi.org/10.1007/s00442-004-1683-3>.
- Shi, Y., Yu, G., 2003. Warm-humid climate and transgressions during 40–30 ka B.P. and their potential mechanisms. *Quat. Sci.* 23 (1), 1–11.
- Si, D., Jiang, D., Hu, A., Lang, X., 2020. Variations in northeast Asian summer precipitation driven by the Atlantic multidecadal oscillation. *Int. J. Climatol.* 41 (3), 1682–1695. <https://doi.org/10.1002/joc.6912>.
- Slivinski, L.C., Compo, G.P., Whitaker, J.S., Sardeshmukh, P.D., Giese, B.S., McColl, C., Allan, R., Yin, X., Vose, R., Titchner, H., Kennedy, J., Spencer, L.J., Ashcroft, L., Brönnimann, S., Brunet, M., Camuffo, D., Cornes, R., Cram, T.A., Crothamel, R., Domínguez-Castro, F., Freeman, J.E., Gergis, J., Hawkins, E., Jones, P.D., Jourdain, S., Kaplan, A., Kubota, H., Le Blancq, F., Lee, T., Lorrey, A., Luterbacher, J., Maugeri, M., Mock, C.J., Moore, G.K., Przybylak, R., Pudmenzky, C., Reason, C., Slonosky, V.C., Smith, C., Tinz, B., Trewin, B., Valente, M.A., Wang, X.L., Wilkinson, C., Wood, K., Wyszyński, P., 2019. Towards a more reliable historical reanalysis: Improvements for version 3 of the Twentieth Century Reanalysis system. *Q. J. R. Meteorol. Soc.* 145 (724), 2876–2908. <https://doi.org/10.1002/qj.3598>.
- Sun, C., Li, J., Zhao, S., 2015. Remote influence of Atlantic multidecadal variability on Siberian warm season precipitation. *Sci. Rep.* 5 (5), 16853. <https://doi.org/10.1038/srep16853>.
- Tao, L., Liang, X., Cai, L., Zhao, J., Zhang, M., 2021. Relative contributions of global warming, AMO and IPO to the land precipitation variabilities since 1930s. *Clim. Dyn.* 56, 2225–2243. <https://doi.org/10.1007/S00382-020-05584-W>.
- Ting, M.F., Kushnir, Y., Seager, R., Li, C.H., 2011. Robust features of Atlantic multidecadal variability and its climate impacts. *Geophys. Res. Lett.* 38 (17), 351–365. <https://doi.org/10.1029/2011GL048712>.

- Trenberth, K.E., Dai, A., van der Schrier, G., Jones, P.D., Barichivich, J., Briffa, K.R., Sheffield, J., 2014. Global warming and changes in drought. *Nat. Clim. Chang.* 4, 17–22.
- van der Schrier, G., Barichivich, J., Briffa, K.R., Jones, P.D., 2013. A scPDSI-based global data set of dry and wet spells for 1901–2009. *J. Geophys. Res. Atmos.* 118 (10), 4025–4048. <https://doi.org/10.1002/jgrd.50355>.
- Wang, B., Ding, Q., 2006. Changes in global monsoon precipitation over the past 56 years. *Geophys. Res. Lett.* 33 (6), L06711. <https://doi.org/10.1029/2005GL025347>.
- Wang, J., Chen, F., Li, Y., Bai, H., 2010. Characteristics of the dry/wet trend over arid Central Asia over the past 100 years. *Clim. Res.* 41 (1), 51–59. <https://doi.org/10.3354/cr00837>.
- Wang, T., Shang, H., Xu, W., Panyushkina, I.P., Mekoc, D.M., Yu, S., Zhang, Q., Jiang, L., Nzabarinda, V., 2021. Tree-ring-based assessments of drought variability during the past 400 years in the Tianshan mountains, arid Central Asia. *Ecol. Indic.* 126, 107702 <https://doi.org/10.1016/j.ecolind.2021.107702>.
- Wu, Z., Huang, N.E., 2009. Ensemble empirical mode decomposition: a noise assisted data analysis method. *Adv. Adapt. Data Anal.* 1 (1), 1–41. <https://doi.org/10.1142/S179353690900047>.
- Yu, L., Gao, Y., Wang, H., Guo, D., Li, S., 2009. The responses of East Asian Summer monsoon to the North Atlantic Meridional Overturning Circulation in an enhanced freshwater input simulation. *Chin. Sci. Bull.* 54, 4724–4732. <https://doi.org/10.1007/s11434-009-0720-3>.
- Zhang, R., Delworth, T.L., 2006. Impact of Atlantic multidecadal oscillations on India/Sahel rainfall and Atlantic hurricanes. *Geophys. Res. Lett.* 33, L17712. <https://doi.org/10.1029/2006GL026267>.
- Zhang, R., Zhang, T., Kelgenbayev, N., He, Q., Maisupova, B., Mambetov, B.T., Chen, F., Dosmanbetov, D., Shang, H., Yu, S., Yuan, Y., 2017. A 189-year tree-ring record of drought for the Dzungarian Alatau, arid Central Asia. *J. Asian Earth Sci.* 148, 305–314. <https://doi.org/10.1016/j.jseas.2017.05.003>.
- Zhang, J., Chen, H., Zhang, Q., 2019. Extreme drought in the recent two decades in northern China resulting from Eurasian warming. *Clim. Dyn.* 52 (5), 2885–2902. <https://doi.org/10.1007/s00382-018-4312-2>.
- Zhang, J., Ma, Q., Chen, H., Zhao, S., Chen, Z., 2021. Increasing warm-season precipitation in Asian Drylands and response to reducing spring snow cover over the Tibetan Plateau. *J. Clim.* 34 (8), 3129–3144. <https://doi.org/10.1175/JCLI-D-20-0479.1>.
- Zhu, K., Guan, X., Huang, J., Wang, J., Guo, S., Cao, C., 2021a. Precipitation over semi-arid regions of North Hemisphere affected by Atlantic Multidecadal Oscillation. *Atmos. Res.* 262 <https://doi.org/10.1016/J.ATMOSRES.2021.105801>.
- Zhu, L., David, J.C., Han, S., Yang, J., Zhang, Y., Li, Z., Zhao, H., Wang, X., 2021b. Influence of the Atlantic Multidecadal Oscillation on drought in northern Daxing'an Mountains, Northeast China. *CATENA*. 198 <https://doi.org/10.1016/J.CATENA.2020.105017>.